Letter

Reorientation-effect measurement of the $\langle 2_1^+ \| \hat{E} 2 \| 2_1^+ \rangle$ matrix element in 36 Ar

J. N. Orce, ^{1,2,*} E. J. Martín Montes, ¹ K. J. Abrahams, ¹ C. Ngwetsheni, ¹ B. A. Brown, ³ M. Kumar Raju, ^{1,4,†} C. V. Mehl, ¹ M. J. Mokgolobotho, ¹ E. H. Akakpo, ^{1,5} D. L. Mavela, ¹ P. Adsley, ^{4,6} R. A. Bark, ⁴ N. Bernier, ^{1,5} T. D. Bucher, ^{1,5} N. R. Erasmus, ¹ T. S. Dinoko, ^{1,4,‡} P. M. Jones, ⁴ N. Y. Kheswa, ⁴ N. A. Khumalo, ^{1,4} E. A. Lawrie, ^{4,1} J. J. Lawrie, ^{4,1} B. L. Lesch, ¹ S. N. T. Majola, ⁵ S. S. Ntshangase, ⁵ P. Papka, ^{4,6} V. Pesudo, ^{1,4} B. Rebeiro, ¹ O. Shirinda, ^{4,8} M. Wiedeking, ^{4,7} and W. Yahia-Cherif, ⁸

¹Department of Physics & Astronomy, University of the Western Cape, P/B X17 Bellville 7535, South Africa

²National Institute for Theoretical and Computational Sciences (NITheCS), Stellenbosch 7535, South Africa

³Department of Physics & Astronomy and National Superconducting Cyclotron Laboratory, Michigan State University,

East Lansing, Michigan 48824-1321, USA

⁴iThemba LABS, National Research Foundation, P.O. Box 722, Somerset West 7129, South Africa

⁵Department of Physics & Engineering, University of Zululand, P/B X1001, KwaDlangezwa 3886, South Africa

⁶Department of Physics, University of Stellenbosch, Private Bag X1, 7602 Matieland, South Africa

⁷School of Physics, University of the Witwatersrand, Johannesburg 2050, South Africa

⁸Université des Sciences, Faculté de Physique, BP 32 El-Alia, 16111 Bab-Ezzouar, Alger, Algeria



(Received 22 September 2021; accepted 28 November 2021; published 16 December 2021)

The spectroscopic quadrupole moment of the first excited 2_1^+ state, $Q_S(2_1^+)$, at 1.970 MeV in 36 Ar was determined at energies well below the Coulomb barrier—where nuclear interference effects are negligible—using the 194 Pt(36 Ar, 36 Ar*) 194 Pt* Coulomb-excitation reaction at 134.2 MeV. Particle-gamma coincidence data were collected using the AFRODITE array—composed of eight high-purity germanium clover detectors—and an upstream double-sided silicon detector at iThemba LABS. A large diagonal matrix element of $\langle 2_1^+ || \hat{E} 2 || 2_1^+ \rangle = 0.163(42)$ *eb* was determined, which yields a more accurate value of $Q_S(2_1^+) = +0.12(3)$ *eb* as compared with previous work, $Q_S(2_1^+) = +0.11(6)$ *eb*, in agreement with modern beyond mean-field and large-scale shell-model calculations. This value is consistent with the ratio of electric quadrupole moments found for other A = 4n self-conjugate nuclei extracted from the reorientation effect and the rotor model, which are surprisingly equivalent to those observed in good rotors in the mass $A \approx 160-180$ region.

DOI: 10.1103/PhysRevC.104.L061305

The spectroscopic or static quadrupole moment, $Q_S(J)$, for an excited state with total angular momentum J provides a measure of the extent to which the nuclear charge distribution in the laboratory frame acquires an ellipsoidal shape [1,2]. It can be determined for states with angular momentum $J \neq 0, \frac{1}{2}$ [3] using the reorientation effect (RE) in Coulomb-excitation reactions, which arises from the hyperfine interaction between Q_S and the time-dependent electric-field gradient generated by the projectile (P) and target (T) during the scattering process. Consequently, the distribution of magnetic substates enhances $(Q_S > 0)$ or suppresses $(Q_S < 0)$ the Coulomb-excitation cross section [1,2]. At energies well below the Coulomb barrier, the RE provides a powerful spectroscopic probe for extracting $\langle 2_1^+ || \hat{E}^2 || 2_1^+ \rangle$ diagonal matrix elements,

which can be directly related to $Q_S(2_1^+)$ [4] by

$$Q_{S}(2_{1}^{+}) = \sqrt{\frac{16\pi}{5}} \frac{1}{\sqrt{2J+1}} \langle JJ20 \mid JJ \rangle \langle 2_{1}^{+} \parallel E2 \parallel 2_{1}^{+} \rangle$$
$$= 0.75793 \langle 2_{1}^{+} \parallel E2 \parallel 2_{1}^{+} \rangle. \tag{1}$$

Assuming an ideal rotor, $Q_S(J)$ is related to the intrinsic quadrupole moment of a nucleus in the body-fixed frame, Q_0 , by

$$Q_S = \frac{3K^2 - J(J+1)}{(2J+3)(J+1)}Q_0,$$
 (2)

where K is the projection of J onto the symmetry axis. For pure K bands, i.e., with no triaxiality, $\gamma=0^\circ$, Q_0 can be determined from the reduced transition probability or $B(E2; J \to J+2)$ value [5]. For $J^\pi=2_1^+$ and K=0, $Q_S(2_1^+)=-\frac{2}{7}Q_0$ and

$$Q_0 = \left(\frac{16\pi}{5}B(E2; 0_1^+ \to 2_1^+)\right)^{1/2}.$$
 (3)

Combining Eqs. (2) and (3) yield the absolute value for the spectroscopic quadrupole moment extracted from the

^{*}coulex@gmail.com; http://nuclear.uwc.ac.za

[†]Present address: Institute of Modern Physics, Chinese Academy of Sciences, Lanzhou 730000, China.

[‡]Present address: National Metrology Institute of South Africa, P/B X 34, Lynnwood Ridge, Pretoria 0040, South Africa.

[§]Present address: Plaatje University, Department of Physical and Earth Sciences, P/B X5008, Kimberley 8301, South Africa.

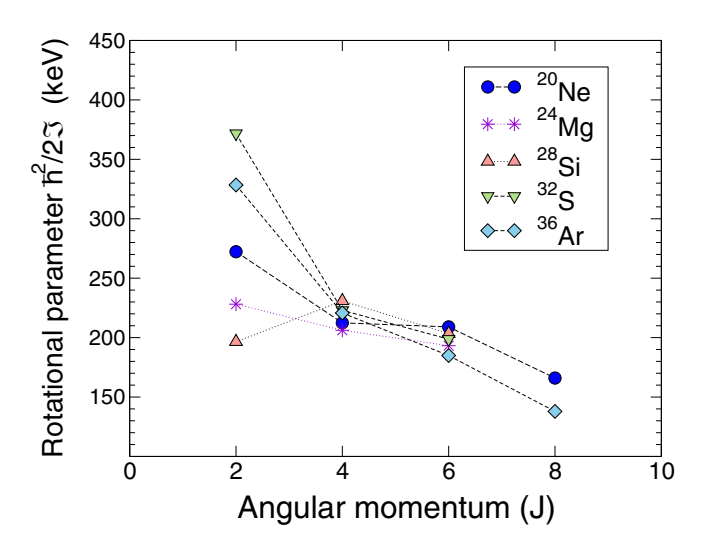


FIG. 1. Rotational parameters $\hbar^2/2\Im$ in 4n self-conjugate *sd*-shell nuclei. Particularly anomalous is the rotational parameter for the 2_1^+ states in 20 Ne, 32 S, and 36 Ar, indicative of shape coexistence.

rotational model, $Q_S(2_1^+)_{B(E2)}$:

$$|Q_S(2_1^+)_{B(E2)}| = 0.9059 B(E2; 0_1^+ \to 2_1^+)^{1/2}.$$
 (4)

Moreover, Q_0 is related to the quadrupole deformation β , to first order, as

$$Q_0 = \left(\frac{16\pi}{5}\right)^{1/2} \frac{3}{4\pi} Z e R^2 \beta, \tag{5}$$

where Z is the proton number and R, the nuclear radius given by $R=1.2A^{1/3}$ fm and $\beta=1.057\delta$, where $\delta=\frac{\Delta R}{R}$ and ΔR is the difference between the semimajor and semiminor axes, respectively parallel and perpendicular to the symmetry axis [5].

A sharp variation of $Q_S(2_1^+)$ values as a function of proton and/or neutron number is found throughout even-even sd-shell nuclei from A=18 to A=40 [6]. The experimentally determined negative $Q_S(2_1^+)$ values in 20 Ne, 24 Mg, and 32 S indicate prolate deformations, whereas positive $Q_S(2_1^+)$ values in 28 Si and 36 Ar represent oblate deformations. An intriguing zig-zag pattern is observed at the end of the sd shell starting from a prolate deformation in 26 Mg and ending with an almost spherical deformation in 40 Ar [6]. With the rapidly changing shell structure in this region, it is not surprising that shape coexistence [7] has recently been identified in 36 Ar [8] and 40 Ca [9] with deformed bands built on the 0_2^+ excitations.

Anomalously high-lying 2_1^+ states that reduces the $E(4_1^+)/E(2_1^+)$ ratio are associated with the mixing of coexisting shapes [7]. Figure 1 shows the rotational parameter $\hbar^2/2\Im$ for a rigid rotor—where $E=\hbar^2/2\Im J(J+1)$ and \Im is the moment of inertia—compared to higher-spin states for A=4n self-conjugate nuclides (i.e., nuclei with equal number of protons and neutrons) in the sd shell between proton and neutron shell closures 8 and 20. The irregular rise of $\hbar^2/2\Im$ at J=2 is particularly pronounced for 36 Ar and 32 S. The general interpretation is that coexisting 0^+ configurations mix and result in a lowering of the binding energy of the nucleus [7]. A simpler scenario is provided by oblate rotational bands

which—with a smaller moment of inertia—may present large $E(2_1^+)$ values. Surprisingly, $Q_S(2_1^+)$ values in some of these nuclides remain poorly determined, particularly for ³⁶Ar [6]. Reasons involve technical aspects such as the difficulty of producing negative ions in tandem accelerators as well as the effect of nuclear interference at high bombarding energies.

An energy ratio of $E(4_1^+)/E(2_1^+) = 2.24$ for 36 Ar is, in principle, consistent with a surface vibration [5]. Nevertheless, an oblate deformation for the 2_1^+ state at 1.970 MeV is indicated by the measured $Q_S(2_1^+) = +0.11(6)$ *e*b of Nakai and co-workers in 1970 [10]. This remains the only RE measurement of the $Q_S(2_1^+)$ value in 36 Ar and the accepted value in the National Nuclear Data Center (NNDC) [11,12]. In these measurements, 36 Ar beams were accelerated to 150 MeV onto a 206 Pb target and particle- γ coincidences collected between a NaI counter (7.5 × 7.5 cm²) and particle counters at 90° and 160° . The quoted $Q_S(2_1^+)$ value by Nakai and co-workers may be questionable because of the minimum separation between nuclear surfaces of $S(\vartheta)_{\min} = 4.3$ fm applied during these experiments, where $S(\vartheta)$ is given by the classical expression

$$S(\vartheta) = D(\vartheta) - (R_p + R_T)$$

$$= \frac{e^2 Z_p Z_T}{8\pi \epsilon_0 T_{\text{lab}}} (1 + A_p / A_T) [1 + \csc(\vartheta / 2)]$$

$$- 1.25 (A_p^{1/3} + A_T^{1/3}) \text{ fm}, \tag{6}$$

with ϑ being the scattering angle in the center-of-mass frame, $\frac{e^2}{4\pi\epsilon_0}=1.44\,$ MeV fm in the Gaussian system and T_{lab} the laboratory kinetic energy in MeV. For negligible interference from nuclear interactions, Spear's systematic study of $Q_S(2_1^+)$ values in the sd shell suggests a safe distance of $S(\vartheta)_{\min} \gtrsim 6.5\,$ fm [6]. Moreover, $Q_S(2_1^+)=+0.0(5)\,|Q_S(2_1^+)_{B(E2)}|\,$ eb in 206 Pb was assumed for the normalization of the 36 Ar data, whereas the currently known value is $Q_S(2_1^+)=+0.17(31)\,|Q_S(2_1^+)_{B(E2)}|\,$ eb [13].

Furthermore, it is interesting to compare the $Q_S(2_1^+)$ value determined using RE and the one extracted from the rotational model [5], $Q_S(2_1^+)_{B(E2)}$ [Eqs. (2) and (3)], by defining the spectroscopic quadrupole ratio [14–16] as

$$r_q := \left| \frac{Q_S(2_1^+)}{Q_S(2_1^+)_{B(E2)}} \right|. \tag{7}$$

Data show $r_q \approx 1$ for good rotors in the $A \approx 160$ –180 mass region, whereas $r_q = 0$ is expected for an ideal vibrator $[Q_S(2_1^+) = 0]$ [5]. With $B(E2; 0_1^+ \to 2_1^+) = 0.0301(16) \ e^2 b^2$ [17] and $Q_S(2_1^+)_{B(E2)} = |0.1572(46)|$ eb, together with $Q_S(2_1^+) = +0.11(6)$ eb, a value of $r_q = 0.70(38)$ is determined for the 2_1^+ state in 36 Ar.

In order to determine the $Q_S(2_1^+)$ value in 36 Ar, a particle- γ coincidence experiment was carried out at iThemba LABS using the 194 Pt(36 Ar, 36 Ar*) 194 Pt* reaction at a safe energy of 134.2 MeV. Beams of 36 Ar7+ at $\approx 1 \times 10^9$ pps bombarded a 96.45% enriched 194 Pt target of 1 mg/cm² thickness in the AFRODITE array [18,19]—composed of eight high-purity germanium clover detectors—coupled to an annular, double-sided CD-type S3 silicon detector (S3 type from Micron Semiconductors [20]) comprising 24 rings and 32 sectors [21] and mounted upstream at 30 mm from the target position and

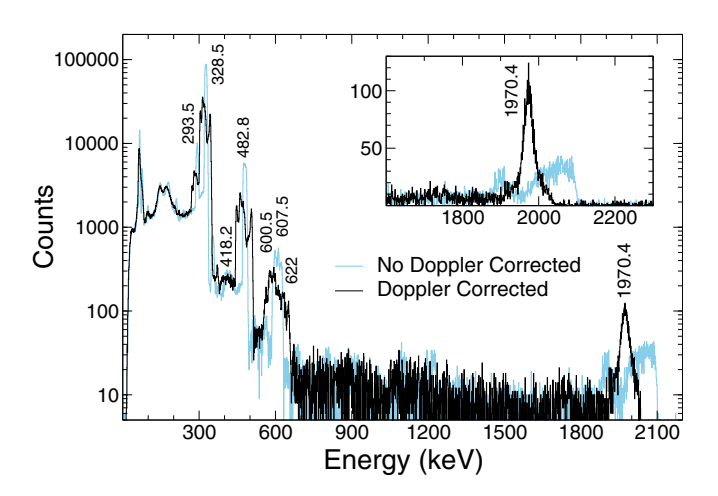


FIG. 2. Doppler (black) and non-Doppler (blue) corrected γ -ray energy spectra in log y scale for the 194 Pt(36 Ar, 36 Ar*) 194 Pt* reaction at 134.2 MeV. The inset shows the 1970.4-keV peaks in 36 Ar with and without Doppler correction in a linear scale.

perpendicularly aligned with the beam axis. The scattering θ angles in the laboratory frame covered between 130.6° and 159.1°, corresponding to $S(\vartheta) \approx 7.1$ and 6.6 fm, respectively. The faces of the clover crystals were positioned at a distance of 19.6 cm from the target, subtending laboratory angles $(\theta_{\gamma}, \phi_{\gamma})$ of $(90^{\circ}, 45^{\circ})$, $(90^{\circ}, 90^{\circ})$, $(90^{\circ}, 225^{\circ})$, $(90^{\circ}, 270^{\circ})$, $(90^{\circ}, 315^{\circ})$, $(135^{\circ}, 0^{\circ})$, $(135^{\circ}, 45^{\circ})$, and $(135^{\circ}, 270^{\circ})$, in a right-handed coordinate system with the z axis downstream of the beam direction. Data were collected using a digital data acquisition (DAQ) system based on 100 MHz Pixie-16 modules from XIA LLC [22].

An optimized sorting code was developed which included faster processing, non-Doppler and Doppler correction, addback, energy sharing, and particle and time tagging conditions. The resulting spectra are shown in Fig. 2. Random subtraction from the prompt particle- γ time spectrum was crucial to remove all background radiation.

The integrated γ -ray yields for the $2^+_1 \to 0^+_1$ 1970.4-and 328.5-keV transitions in 36 Ar and 194 Pt, respectively, have been analyzed using the semiclassical coupled-channel Coulomb-excitation least-squares code GOSIA [23]. The use of the semiclassical approximation is justified from Rutherford scattering cross sections and the Sommerfeld parameter, $\eta = \frac{a}{\lambda} \approx 115 \gg 1$, where a is the half distance of closest approach in a head-on collision and λ is the de Broglie wavelength. Calculations consider the known spectroscopic information such as level lifetimes, branching ratios and matrix elements, kinematics, detector geometry, and beam energy losses. The effect of higher-lying states in the evaluation of $\langle 2^+_1 \| \hat{E} \hat{Z} \| 2^+_1 \rangle$ in 36 Ar was estimated using GOSIA and considered negligible (<0.1%).

Figure 3 shows the experimental and theoretical heavy-ion angular distribution of yields in the laboratory frame, integrated over eight clover detectors, for the $2^+_1 \rightarrow 0^+_1$ transitions in $^{194}{\rm Pt}$ (a) and $^{36}{\rm Ar}$ (b). The angular distributions predicted by GOSIA for both $^{194}{\rm Pt}$ and $^{36}{\rm Ar}$ are in good agreement with experimental yields. Predictions of the cross sections for

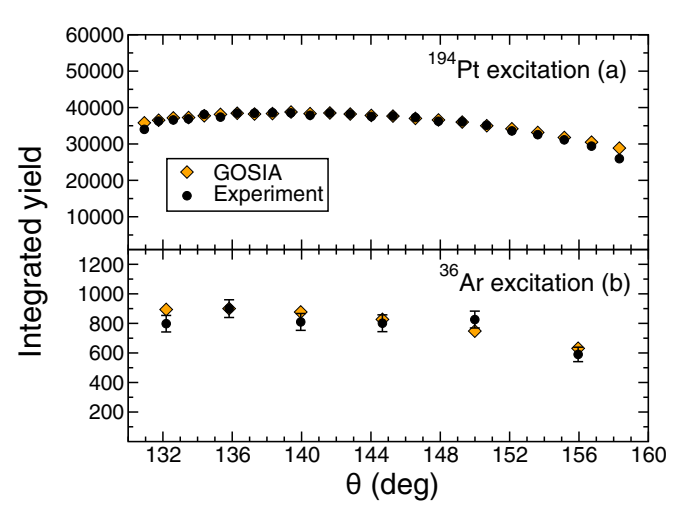


FIG. 3. Heavy-ion angular distributions showing experimental and calculated integrated γ -ray yields as a function of laboratory scattering angle, θ , for the deexcitation of the 2_1^+ states in (a) 194 Pt and (b) 36 Ar.

populating states in 36 Ar were calculated at fixed values of $\langle 2_1^+ \| \hat{E}^2 \| 0_1^+ \rangle = 0.1735$ eb [17] and $\langle 2_1^+ \| \hat{E}^2 \| 2_1^+ \rangle = +0.163$ eb (the intersection point of the centroid of the two bands in Fig. 4, as explained below) and normalized to the experimental yields with a common normalization factor.

The normalization procedure used in Refs. [24,25] was applied to determine $\langle 2_1^+ \| \hat{E}^2 \| 2_1^+ \rangle$, where Coulomb-excitation curves are determined in the $\langle 2_1^+ \| \hat{E}^2 \| 2_1^+ \rangle - \langle 2_1^+ \| \hat{E}^2 \| 0_1^+ \rangle$ plane. The $\langle 2_1^+ \| \hat{E}^2 \| 0_1^+ \rangle$ transitional matrix element is the first order in Coulomb-excitation perturbation theory and is related to the reduced transition probability $B(E2; 0_1^+ \to 2_1^+)$ as

$$B(E2; 0_1^+ \to 2_1^+) = |\langle 2_1^+ || \hat{E2} || 0_1^+ \rangle|^2.$$
 (8)

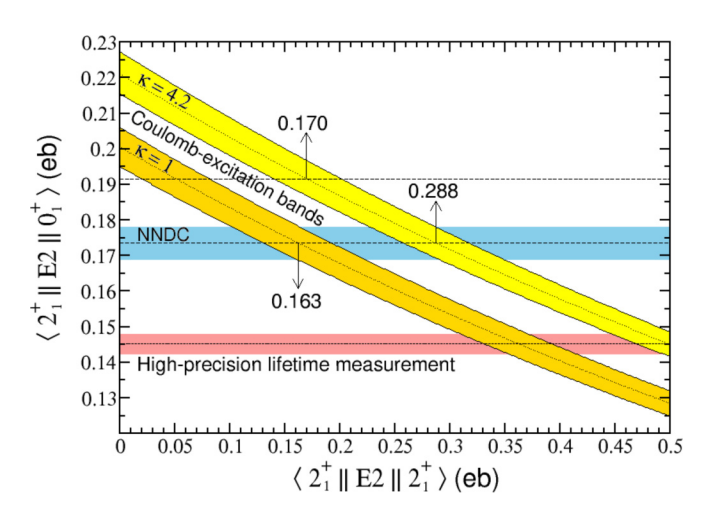


FIG. 4. The Coulomb-excitation bands show the variation of $\langle 2_1^+ \| \hat{E} 2 \| 0_1^+ \rangle$ as a function of $\langle 2_1^+ \| \hat{E} 2 \| 2_1^+ \rangle$ in 36 Ar for $k(2_1^+) = 1$ and $k(2_1^+) = 4.2$. The horizontal bands represents the 1σ boundary for $\langle 2_1^+ \| \hat{E} 2 \| 0_1^+ \rangle = 0.1735(46)$ *eb* [17] and $\langle 2_1^+ \| \hat{E} 2 \| 0_1^+ \rangle = 0.1453(28)$ *eb* [33].

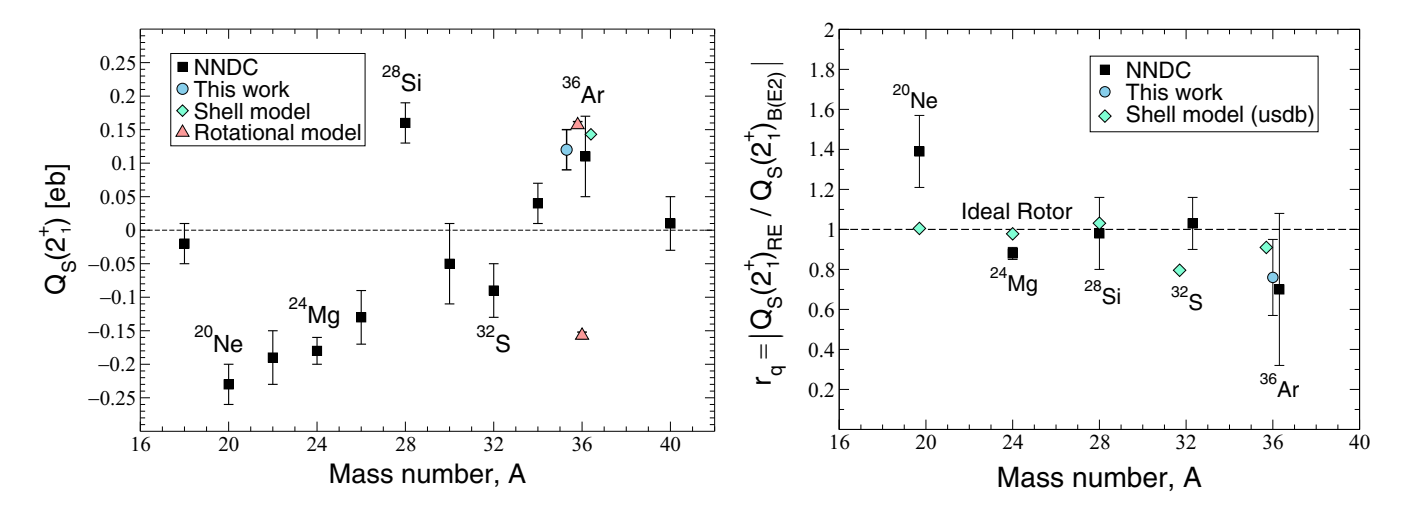


FIG. 5. $Q_S(2_1^+)$ (left) and r_q (right) values determined in the sd shell, including our new results for 36 Ar, $Q_S(2_1^+) = +0.12(3)$ eb and $r_q = 0.76(19)$.

Each data point in the Coulomb-excitation curves was determined by fixing $\langle 2_1^+ \| \hat{E} 2 \| 2_1^+ \rangle$ in steps of 0.01 *e*b, and varying $\langle 2_1^+ \| \hat{E} 2 \| 0_1^+ \rangle$ until converging with the experimental intensity ratio between target and projectile, I_x^- / I_y^P , given by

$$\frac{\sigma_{E2}^T W(\vartheta)^T}{\sigma_{F2}^P W(\vartheta)^P} = 1.037 \frac{N_{\gamma}^T}{N_{\gamma}^P} \frac{\varepsilon_{\gamma}^P}{\varepsilon_{\gamma}^T} = \frac{I_{\gamma}^T}{I_{\gamma}^P}.$$
 (9)

Here, $W(\vartheta)$ represents the integrated angular distribution of the deexcited γ rays in coincidence with the inelastic scattered particles [26], and the factor 1.037 accounts for the 96.45% enrichment of the ¹⁹⁴Pt target chosen for normalization. Relative efficiencies of $\varepsilon_{\gamma}^{P}=152(5)$ and $\varepsilon_{\gamma}^{T}=409(8)$, and total counts of $N_{\gamma}^{P}=4725(103)$ and $N_{\gamma}^{T}=860471(961)$ for the 1970.4- and 328.5-keV γ -ray transitions, respectively, yield $I_{\gamma}^{T}/I_{\gamma}^{P}=65(3)$. The quoted error on this measurement arises from the uncertainties of N_{γ}^{P} (2.2%) and ε_{γ}^{P} (3.0%).

The resulting Coulomb-excitation diagonal band is shown on the left of Fig. 4 (orange band), where the dashed line is the central value and the two solid lines correspond to the 1σ loci limits. The horizontal band represents the accepted value in the NNDC, $\langle 2_1^+ \| \hat{E}^2 \| 0_1^+ \rangle = 0.1735(46)~eb~[17]$. In principle, this horizontal band should be extracted from independent measurements rather than Coulomb excitation, although we opted to use the more precise NNDC value because of its agreement [27] with the weighted average determined from previous lifetime measurements, $\langle 2_1^+ \| \hat{E}^2 \| 0_1^+ \rangle = 0.1738(75)~eb~[28–32]$.

We have discarded a previous high-precision lifetime measurement [33] [$\tau=0.65(2)$ ps] since it is several standard deviations from the 2001 evaluation of $B(E2;0_1^+\to 2_1^+)$ values [34] and is also neglected in the 2016 evaluation [17]. Moreover, this high-precision lifetime yields $\langle 2_1^+ || \hat{E}^2 || 0_1^+ \rangle = 0.1453(28)$ *e*b, which as shown by the lower horizontal band in Fig. 4, gives rise to an anomalously large oblate deformation. Further discrepancies between similar high-precision lifetime measurements [35,36] and Coulomb-excitation studies [34,37] have been found when complicated

targets/stopping powers are involved in the Doppler-shift attenuation method (DSAM) analysis.

Assuming a nominal polarizability parameter of $\kappa(2_1^+)=1$ [38], where κ indicates deviations from the actual polarization effect of the giant dipole resonance compared to that predicted by the hydrodynamic model [39], a positive value of $\langle 2_1^+ \| \hat{E}^2 \| 2_1^+ \rangle = +0.163(42)$ eb is obtained from the intersection of the two bands, corresponding to $Q_S(2_1^+)=+0.12(3)$ eb and $Q_0=-0.42(11)$ eb, which yields a large oblate quadrupole deformation of $\beta=-0.20(5)$. The uncertainty of $\langle 2_1^+ \| \hat{E}^2 \| 2_1^+ \rangle$ is determined from the overlap region between the two bands assuming central values for the $\langle 2_1^+ \| \hat{E}^2 \| 0_1^+ \rangle$ band, ± 0.03 eb, and the Coulomb-excitation diagonal curve, ± 0.03 eb, added in quadrature. This result is in agreement with previous work [10], but it presents a higher precision. The improvement is clearly seen in Fig. 5.

A zig-zag pattern of $Q_S(2_1^+)$ values remains at the end of the sd shell, as shown in Fig. 5. Within the simple pairing-coupling scheme [40], a prolate deformation is expected at the beginning of the shell as particles start filling up the empty shells, whereas a flip over is expected after midshell, where holes in the filled shells align their orbits along the polar axis and give rise to oblate deformations. Towards the end of the shell, the dominant pairing of holes restores the spherical shape.

In more detail, the sign of $Q_S(2_1^+)$ values in A = 4n self-conjugate nuclei between the A = 16 and A = 40 shell closures—including the zig-zag pattern at the end of the sd shell—can be explained with a modified Nilsson model [41]. Figure 6 shows proton and neutron single-particle energies for 36 Ar in an axially deformed Woods-Saxon potential as a function of deformation along the Fermi surface. It is evident that an oblate deformation is favored from the relatively more bound single-particle energies. A similar qualitative interpretation can be provided for other nuclei in the sd shell.

Additionally, our results are supported by modern beyond-mean-field (BMF) calculations [42–44], which yield $Q_S(2_1^+)_{\text{theory}} = +0.13 \ e\text{b}$ and with the magnitude predicted by the rotor model, $Q_S(2_1^+)_{B(E2)} = |0.157(5)| \ e\text{b}$. Interestingly,

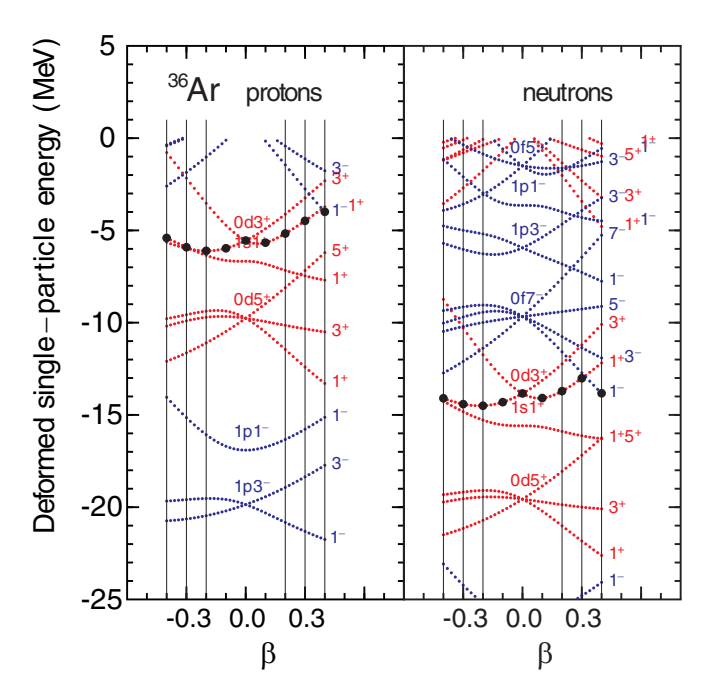


FIG. 6. Modified Nilsson diagram for ³⁶Ar showing lower single-particle energies for oblate deformations along the Fermi surface [41].

when combined with previous work [11], a consistent pattern of r_q values emerges for A=4n self-conjugate nuclei in the sd shell with $r_q \approx 1$, i.e., analogous to those observed for well-deformed rotors in the $A \approx 160$ –180 mass region [16].

Shell-model (SM) calculations of r_q values were performed in this work using the *usdb* [45] and *usdc* [46] interactions, and the code NUSHELLX [47,48]. Identical results were obtained, and are shown in the right panel of Fig. 5 (diamonds). A constant value of $r_q \approx 1$ is calculated from ²⁰Ne to midshell ²⁸Si with slightly lower values for ³²S and ³⁶Ar. Curiously, Stone's evaluation of $Q_S(2_1^+)$ values [12] considers for ³²S the latest measurement, $Q_S(2_1^+) = -0.16(2)$ *eb*, by Vermeer and co-workers in 1982 [49], which yields $r_q = 1.03(13)$. If one considers all RE measurements [49–55], a more accurate weighted value of $Q_S(2_1^+) = -0.12(1)$ *eb* is determined, which should be the accepted value in the NNDC, and yields $r_q = 0.77(6)$, in agreement with SM calculations.

Additional SM calculations were carried out with the code OXBASH [56] in order to determine the nuclear polarizability of the ground and 2_1^+ states in 36 Ar using the wbp interaction [57] in the spsdpf model space and considering the formalism in Ref. [58]. Calculations yield $\kappa(g.s.) = 1.65$ and $\kappa(2_1^+) = 4.2$. Although there are no photoabsorption data available for 36 Ar to compare with, $\sigma(\gamma, p)$ and $\sigma(\gamma, n)$ contributions for other self-conjugate nuclei [59] are known to present values

of $\kappa(g.s.) > 1$ [60]. More details about these SM calculations will be presented in a separate paper [61]. Assuming $\kappa(2_1^+) = 4.2$, the Coulomb-excitation band shifts the crossing with the $\langle 2_1^+ \| \hat{E} 2 \| 0_1^+ \rangle$ horizontal band [17] towards a more pronounced oblate deformation, $\langle 2_1^+ \| \hat{E} 2 \| 2_1^+ \rangle = +0.288(42)$ eb, with respect to rotor model, SM, and BMF predictions.

A large $\kappa > 1$ polarizability is found to affect Coulomb-excitation measurements of collective properties in self-conjugate nuclides [25,62]. One interesting possibility arises from the comparison of previous measurements in 36 Ar. The recent lifetime measurement of the 2_1^+ state in 36 Ar [32] was determined using the DSAM following Coulomb excitation, and yields an E2 strength in agreement with previous inelastic electron scattering (e, e') [63] and Coulomb-excitation measurements [10,64,65], which seems to reconcile a long-standing \approx 20% deviation between previous Coulomb-excitation [10,64,65] and lifetime [28–31] measurements.

Although such a discrepancy seems to be resolved, a larger weighted average of $\langle 2_1^+ \| \hat{E}2 \| 0_1^+ \rangle = +0.1915(136)$ *eb* is determined if one considers only the accepted lifetimes prior to 2017 [28–31] (top dashed line in Fig. 4), which crosses the $\kappa(2_1^+)=4.2$ Coulomb-excitation band at $\langle 2_1^+ \| \hat{E}2 \| 2_1^+ \rangle = +0.170$ *eb*; i.e., a value similar to the one quoted assuming $\kappa=1$ and the accepted NNDC value [17], but closer to $r_q=1$. Both Coulomb-excitation and the recent DSAM analyses might suffer from having a large $\kappa(2_1^+)=4.2$; particularly when the latter measurement utilized stopping powers corrected by the Coulomb-excitation scattering process [32].

In conclusion, the Coulomb-excitation analysis performed in this work yields the most accurate determination of $\langle 2_1^+ || \hat{E} \hat{2} || 2_1^+ \rangle = +0.163(42)$ eb in ³⁶Ar from particle- γ coincidence data collected at iThemba LABS using the AFRODITE array and a double-sided silicon detector at very safe distances. Such an oblate deformation is in agreement with the pairing-coupling, the modified Nilsson, and the rotor models as well as BMF and SM calculations. Overall, a similar r_q trend is observed between A = 4n self-conjugate and well-deformed rotors in heavy nuclei. The growing indication of an increasing nuclear polarizability with excitation energy could be tested with a precise lifetime measurement of the 2^{+}_{1} state in ³⁶Ar, without involving Coulomb excitation. A precise lifetime measurement can reduce the uncertainty associated with $\langle 2_1^+ || \hat{E} 2 || 0_1^+ \rangle$ in determining the relevant $\langle 2_1^+ || \hat{E} 2 || 2_1^+ \rangle$ matrix element.

We acknowledge the accelerator group at iThemba LABS for masterful delivery of ³⁶Ar beams. This work was supported by the South Africa's National Research Foundation (NRF) under Grant No. 93500, the SANHARP program, the National Science Foundation (NSF) under Grants No. PHY-1811855 and No. PHY-2110365, the SA-CERN Collaboration, and the MANuS/MatSci Honours/Masters program.

^[1] J. de Boer and J. Eichler, Adv. Nucl. Phys. 1, 1 (1968).

^[2] O. Häusser, in *Nuclear Spectroscopy and Reactions, Part C*, edited by J. Cerny (Academic Press, New York, 1974).

^[3] A. deShalit and H. Feshbach, Theoretical Nuclear Physics, Volume 1: Nuclear Structure (Wiley-Blackwell, New York, 1974).

- [4] K. Alder and A. Winther, *Electromagnetic Excitation* (North-Holland, Amsterdam, 1975).
- [5] A. Bohr and B. R. Mottelson, *Nuclear Structure*, *Volume II* (World Scientific, Singapore, 1998).
- [6] R. H. Spear, Phys. Rep. 73, 369 (1981).
- [7] K. Heyde and J. L. Wood, Rev. Mod. Phys. 83, 1467 (2011).
- [8] C. E. Svensson, E. Caurier, A. O. Macchiavelli, A. Juodagalvis, A. Poves, I. Ragnarsson, S. Aberg, D. E. Appelbe, R. A. E. Austin, C. Baktash, G. C. Ball, M. P. Carpenter, E. Caurier, R. M. Clark, M. Cromaz, M. A. Deleplanque, R. M. Diamond, P. Fallon, M. Furlotti, A. Galindo-Uribarri, R. V. F. Janssens, G. J. Lane, I. Y. Lee, M. Lipoglavsek, F. Nowacki, S. D. Paul, D. C. Radford, D. G. Sarantites, D. Seweryniak, F. S. Stephens, V. Tomov, K. Vetter, D. Ward, and C. H. Yu, Phys. Rev. Lett. 85, 2693 (2000).
- [9] E. Ideguchi, D. G. Sarantites, W. Reviol, A. V. Afanasjev, M. Devlin, C. Baktash, R. V. F. Janssens, D. Rudolph, A. Axelsson, M. P. Carpenter, A. Galindo-Uribarri, D. R. LaFosse, T. Lauritsen, F. Lerma, C. J. Lister, P. Reiter, D. Seweryniak, M. Weiszflog, and J. N. Wilson, Phys. Rev. Lett. 87, 222501 (2001).
- [10] K. Nakai, F. S. Stephens, and R. M. Diamond, Phys. Lett. B 34, 389 (1971).
- [11] https://www.nndc.bnl.gov/ensdf/
- [12] N. J. Stone, At. Data Nucl. Data Tables 111-112, 1 (2016).
- [13] A. M. R. Joye, A. M. Baxter, S. Hinds, D. C. Kean, and R. H. Spear, Phys. Lett. B 72, 307 (1978).
- [14] S. J. Q. Robinson, A. Escuderos, L. Zamick, P. von Neumann-Cosel, A. Richter, and R. W. Fearick, Phys. Rev. C 73, 037306 (2006).
- [15] S. Yeager and L. Zamick, arXiv:0807.4679.
- [16] Y. Y. Sharon, N. Benczer-Koller, G. J. Kumbartzki, L. Zamick, and R. F. Casten, Nucl. Phys. A **980**, 131 (2018).
- [17] B. Pritychenko, M. Birch, M. Horoi, and B. Singh, At. Data Nucl. Data Tables 107, 1 (2016).
- [18] J. F. Sharpey-Schafer, Nucl. Phys. News 14, 3 (2004).
- [19] M. Lipoglavšek et al., Nucl. Instrum. Methods A 557, 523 (2007).
- [20] http://79.170.44.80/micronsemiconductor.co.uk/wp-content/uploads/2017/01/cat.pdf
- [21] A. N. Ostrowski, S. Cherubini, T. Davinson, D. Groombridge, A. M. Laird, A. Musumarra, A. Ninane, A. Di Pietro, A. C. Shotter, and P. J. Woods, Nucl. Instrum. Methods A 480, 448 (2002).
- [22] https://xia.com/
- [23] T. Czosnyka, D. Cline, and C. Y. Wu, Bull. Am. Phys. Soc. 28, 745 (1983).
- [24] J. N. Orce, T. E. Drake, M. K. Djongolov, P. Navratil, S. Triambak, G. C. Ball, H. AlFalou, R. Churchman, D. S. Cross, P. Finlay, C. Forssen, A. B. Garnsworthy, P. E. Garrett, G. Hackman, A. B. Hayes, R. Kshetri, J. Lassen, K. G. Leach, R. Li, J. Meissner, C. J. Pearson, E. T. Rand, F. Sarazin, S. K. L. Sjue, M. A. Stoyer, C. S. Sumithrarachchi, C. E. Svensson, E. R. Tardiff, A. Teigelhoefer, S. J. Williams, J. Wong, and C. Y. Wu, Phys. Rev. C 86, 041303(R) (2012).
- [25] M. K. Raju et al., Phys. Lett. B. 777, 250 (2018).
- [26] K. Adler, A. Bohr, T. Huus, B. Mottelson, and A. Winther, Rev. Mod. Phys. 28, 432 (1956).
- [27] M. Birch, B. Pritychenko, and B. Singh, Nucl. Phys. A 955, 145 (2016).
- [28] H. Grawe and K. P. Lieb, Nucl. Phys. A 127, 13 (1969).

- [29] J. P. Thibaud, M. M. Aléonard, D. Castera, Ph. Hubert, F. Leccia, and P. Mennrath, J. Phys. (Paris) 31, 131 (1970).
- [30] G. A. Hokken, J. A. J. G. Hendricx, and J. de Kogel, Nucl. Phys. A 194, 481 (1972).
- [31] P. M. Johnson, M. A. Meyer, and D. Reitmann, Nucl. Phys. A 218, 333 (1974).
- [32] P. Voss, T. E. Drake, K. Starosta, C. Andreoiu, R. Ashley, G. C. Ball, P. C. Bender, A. Chester, R. Churchman, D. S. Cross, A. B. Garnsworthy, G. Hackman, B. Hadinia, R. Henderson, B. Jigmeddorj, S. Ketelhut, R. Krucken, A. T. Laffoley, K. G. Leach, D. Miller, R. Orlandi, C. J. Pearson, J. Pore, M. M. Rajabali, E. T. Rand, C. E. Svensson, E. Tardiff, C. Unsworth, Z. M. Wang, and A. Signoracci, Phys. Rev. C 96, 024305 (2017).
- [33] K.-H. Speidel, S. Schielke, J. Leske, J. Gerber, P. Maier-Komor, S. J. Q. Robinson, Y. Y. Sharon, and L. Zamick, Phys. Lett. B 632, 207 (2006).
- [34] S. Raman, C. W. Nestor, Jr., C. W. Nestor, and P. Tikkanen, At. Data Nucl. Data Tables 78, 1 (2001).
- [35] O. Kenn, K.-H. Speidel, R. Ernst, J. Gerber, N. Benczer-Koller, G. Kumbartzki, P. Maier-Komor, and F. Nowacki, Phys. Rev. C 63, 021302(R) (2000).
- [36] O. Kenn, K.-H. Speidel, R. Ernst, J. Gerber, P. Maier-Komor, and F. Nowacki, Phys. Rev. C 63, 064306 (2001).
- [37] J. M. Allmond, B. A. Brown, A. E. Stuchbery, A. Galindo-Uribarri, E. Padilla-Rodal, D. C. Radford, J. C. Batchelder, M. E. Howard, J. F. Liang, B. Manning, R. L. Varner, and C.-H. Yu, Phys. Rev. C 90, 034309 (2014).
- [38] J. N. Orce, Phys. Rev. C 91, 064602 (2015).
- [39] A. Migdal, J. Exp. Theor. Phys. U.S.S.R. 15, 81 (1945).
- [40] D. J. Rowe, Nuclear Collective Motion (Methuen and Co. Ltd., London, 1970).
- [41] S. Cwiok, J. Dudek, W. Nazarewicz, J. Skalski, and T. Werner, Comput. Phys. Commun. 46, 379 (1987).
- [42] R. R. Rodriguez-Guzman, J. L. Egido, and L. M. Robledo, Phys. Lett. B 474, 15 (2000).
- [43] E. Caurier, F. Nowacki, and A. Poves, Phys. Rev. Lett. 95, 042502 (2005).
- [44] M. Bender, H. Flocard, and P.-H. Heenen, Phys. Rev. C 68, 044321 (2003).
- [45] W. A. Richter, S. Mkhize, and B. A. Brown, Phys. Rev. C 78, 064302 (2008).
- [46] A. Magilligan and B. A. Brown, Phys. Rev. C **101**, 064312 (2020).
- [47] W. D. M. Rae, NuShellX, http://www.garsington.eclipse.co.uk.
- [48] B. A. Brown and W. D. M. Rae, Nucl. Data Sheets 120, 115 (2014).
- [49] W. J. Vermeer, M. T. Esat, and R. H. Spear, Nucl. Phys. A 389, 185 (1982).
- [50] K. Nakai, J. L. Quebert, F. S. Stephens, and R. M. Diamond, Phys. Rev. Lett. 24, 903 (1970).
- [51] O. Häusser, T. K. Alexander, A. B. McDonald, and W. T. Diamond, Nucl. Phys. A 175, 593 (1971).
- [52] A. Olin, O. Häusser, T. K. Alexander, A. J. Ferguson, and W. Witthuhn, Nucl. Phys. A 221, 555 (1974).
- [53] G. C. Ball, O. Häusser, T. K. Alexander, W. G. Davies, J. S. Foster, I. V. Mitchell, J. R. Beene, D. Horn, and W. McLatchie, Nucl. Phys. A 349, 271 (1980).
- [54] G. Dannhauser, J. de Boer, R. Lutter, F. Riess, and H. Bohn, Z. Phys. A 300, 71 (1981).
- [55] L. D. Mavela, https://etd.uwc.ac.za/handle/11394/7334

- [56] B. A. Brown et al., MSU-NSCL Report No. 1289 (unpublished).
- [57] E. K. Warburton and B. A. Brown, Phys Rev. C 46, 923 (1992).
- [58] J. N. Orce, Int. J. Mod. Phys. E **29**, 2030002 (2020).
- [59] R. A. Eramzhyan, B. S. Ishkhanov, I. M. Kapitonov, and V. G. Neudatchin, Phys. Rep. 136, 229 (1986).
- [60] C. Ngwetsheni, M.Sc. thesis, 2019 (unpublished), https://etd. uwc.ac.za/handle/11394/6705
- [61] C. Ngwetsheni, J. N. Orce, T. Nogwanya, and B. A. Brown (unpublished).
- [62] C. V. Mehl et al. (unpublished).
- [63] J. M. Finn, H. Crannell, P. L. Hallowell, J. T. O'Brien, and S. Penner, Nucl. Phys. A 290, 99 (1977).
- [64] P. D. Cottle, M. Fauerbach, T. Glasmacher, R. W. Ibbotson, K. W. Kemper, B. Pritychenko, H. Scheit, and M. Steiner, Phys. Rev. C 60, 031301(R) (1999).
- [65] B. V. Pritychenko et al., Phys. Lett. B 461, 322 (1999); 467, 309(E) (1999).